Simulation modeling and electron energy distribution function studies of an electron cyclotron resonance source with a new magnetic topology

A. Khandelwal* and J.-E. Ducret
Grand Accélérateur National d'Ions Lourds, Bd. Henri Becquerel, CS 55027, F-14076 Caen, France

L. Maunoury
Normandy Hadrontherapy, rue Claude Bloch, F-14000 Caen, France

L. Garrigues
LAPLACE, Université de Toulouse, INPT, UPS, F-31062 Toulouse, France

(Received 6 February 2023; accepted 7 September 2023; published 10 October 2023)

A 10 GHz ECR ion source (PK-GANESA) with a new magnetic field topology was developed in a GANIL-Pantechnik collaboration. The performance of this source is analyzed through simulations of electron trajectories over a time of 20 μs to ensure both rf-heating and magnetic confinement, using the code TrapCAD. The electron energy distribution functions obtained from the simulations are characterized with respect to radio frequency, heating power, and simulation time. The results are compared with a more traditional 10 GHz ECR source (NANOGANIII) presently used at GANIL. Our study demonstrates an improvement of electron confinement (a factor 10 increase) with increasing rf heating power which should in principle lead to the production of highly charged ions, at variance with the measured production of high-charge-state ions, significantly lower than for the NANOGANIII source. A tentative explanation of the difference between both sources is discussed.

DOI: 10.1103/PhysRevAccelBeams.26.103501

I. INTRODUCTION

A. Context of the work

GANIL (Grand Accélérateur National d'Ions Lourds) is one of the few laboratories in the world providing stable and radioactive ion beams for physicists to probe nuclear matter and improve our understanding of the atomic nucleus and its properties. The facility consists of cyclotrons for producing stable beams which can either be used directly for experiments or can be injected into the SPIRAL1 [1] set up to produce radioactive-ion beams, as well as a new superconducting linear accelerator SPIRAL2 [2]. A wide spectrum of beams (from proton and neutron to ^{238}U) with energies ranging from a few eV up to almost 100 MeV per nucleon are available for experiments.

Ion beams are produced in sources prior to their acceleration; for high-energy beams, high-charge-state (HCS) ions are required as an output of the injectors. GANIL has traditionally used low-pressure off-balance ion sources based on the ECR heating process for feeding the accelerators with multicharged ions [3]. One of the challenges of this type of source is to produce HCS metallic ion beams, with intensity and stability corresponding to the requirements of nuclear-physics experiments.

There are several drawbacks in conventional ECR ion sources [4]. The use of multipole magnets results in a star-shaped beam, which leads to particle loss due to the lack of axial symmetry. A portion of the beam must be cut off during extraction and transport of the homogeneous core, to match the acceptance of the low-energy beam line of the accelerator. The use of magnetic coils is also a limitation for high-frequency design (above 18 GHz) due to mechanical constraints, since the use of superconducting magnets generates high field-strength at the edges. To overcome this, a new kind of axisymmetric ion source, based on permanent magnets, has been designed by a GANIL-Pantechnik collaboration called PK-GANESA and tested to produce Argon ions [5]. It is an extension of the MONO1000 ion source (operating at 2.45 GHz) devoted to producing mainly monocharged ions [6]. By increasing the operating frequency up to 10 GHz, plasma density, as well as average electron temperature, must increase such as to generate HCS. Figure 1 displays the comparison of the measured mass-over-charge spectra for a standard 10 GHz ECR ion source NANOGANIII, MONO1000, and PK-GANESA [5]. Curves have been

*arpan.khandelwal@ganil.fr
Also at LAPLACE, Université de Toulouse, INPT, UPS, F-31062 Toulouse, France.

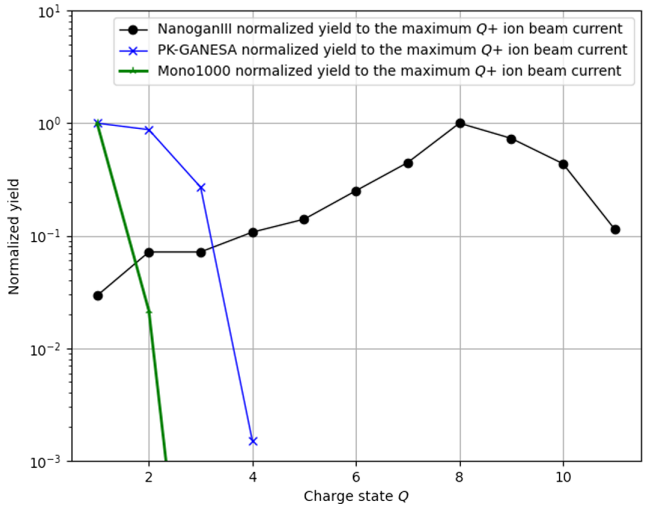

FIG. 1. Charge state distribution of Ar ions normalized to the maximum current peak for NANOGANIII (black, a maximum peak current of 150 μA [8]); PK-GANESA (blue, maximum peak current of 190 μA [5]); and MONO1000 (green, maximum peak current of 501 μA).

normalized to the maximum current peak of each charged-state distribution. NANOGANIII produces much higher charge state ions than PK-GANESA which is more efficient than MONO1000. The newly-designed ion source seems unable to produce HCS ions as compared with NANOGANIII. As shown in [7], the plasma of MONO1000 is hollow and exhibits higher densities off the symmetry axis of the source, i.e., closer to the resonance zone where the heating of the electrons should in principle lead to an efficient ionization of the atoms and ions because of the magnetic confinement. This should also be the case for PK-GANESA. The design of PK-GANESA is a continuation of the MONO1000 ion-source family [6] operating at 2.45 GHz, which delivers single-charge and light-mass ion currents. Hence the poor performances of PK-GANESA happened to be unexpected.

To understand the measurements on PK-GANESA, a numerical investigation has been carried out, aiming at characterizing the Electron Energy Distribution Functions (EEDF) of PK-GANESA as compared with those of NANOGANIII in absence of collisions. Such a comparison has the goal of investigating the role of the magnetic topology of the new design PK-GANESA with respect to NANOGANIII's during electron heating by the microwave.

In the present paper, the collision-less heating of the electrons by the 10-GHz microwave is considered through two questions: (1) What are the initial locations of the electrons which lead to longer confinement and larger heating (higher average energies)? (2) What are the electron energy spectra obtained after "long times" in the timescale of the phenomena at play? Throughout this paper, the comparison between both sources is detailed, to underline the role of the magnetic topology of PK-GANESA. In the first part, the topology of the magnetic field of PK-GANESA is compared with the standard-design ECRIS NANOGANIII's. In the second part, TrapCAD [9] simulations are described, and the results obtained for different variables (electron energy or spatial distributions, electron loss rates) are presented. In the third part of the study, SIMION [10] calculations are shown and analyzed, with the aim of estimating the ion trajectories exiting the source. The fourth part provides a summary and conclusions.

B. Magnetic field topologies

The present generation of standard ECR ion sources, such as NANOGANIII use a combination of solenoids (axial magnetic field) and multipole magnets (radial magnetic field) for creating the magnetic topology to trap the charged particles of the plasma and generate HCS ions. Such a magnetic topology results in a "pill-shaped" electron cyclotron resonance surface as shown in Figs. 2(a) and 2(c) for a radio frequency (rf) microwave of 10 GHz (red lines) with a resonant magnetic field value of 0.3751 T. The ECR resonance zone is the region where the incoming rf is close to the cyclotron frequency of the electrons. In that volume, it has been established clearly that the highly charged ions are created and trapped together with the hot electrons. In the resonance zone, magnetic-field lines exhibit a complex structure, following the sextupolar symmetry of the field, with nodes. As can be seen in Fig. 2(a), the magnetic field lines connect the mid-plane with the source's injection and exit holes. In Refs. [11,12], Spädtke *et al.* established the relationship between magnetic field lines and extracted highly charged ions. Those magnetic field lines (as in our example displayed for the NANOGANIII ion source, the yellow lines), connect the ECR zones, where multicharged ions are produced to the extraction aperture.

The new source PK-GANESA has a completely axi-symmetric magnetic configuration (defining axial and radial magnetic fields) to generate a rather simpler and completely different magnetic topology, see Fig. 1(a) of [5]. To illustrate the comparison between the two sources, we show in Fig. 2(a) for NANOGANIII and Fig. 2(b) for PK-GANESA the magnetic-field-line topology, which are basically different, in particular because these field lines remain parallel to the source axis for PK-GANESA in the inner part of the volume to end up on the chamber wall. This is not the case for NANOGANIII for which lines connect this inner volume to its exits. This new magnetic configuration results in a "dumbbell-shaped" resonance surface [Figs. 2(c) and 2(d)]. Combined with the property of the field lines to remain off-axis, where the magnetic field is smaller, this seems more favorable to maintain the ions in the vicinity of the resonance zone and therefore, to optimize collisions with the hot electrons and produce higher charge-states via step wise ionisztion. Figures 2(e) and 2(f) show the magnetic field transverse distribution at

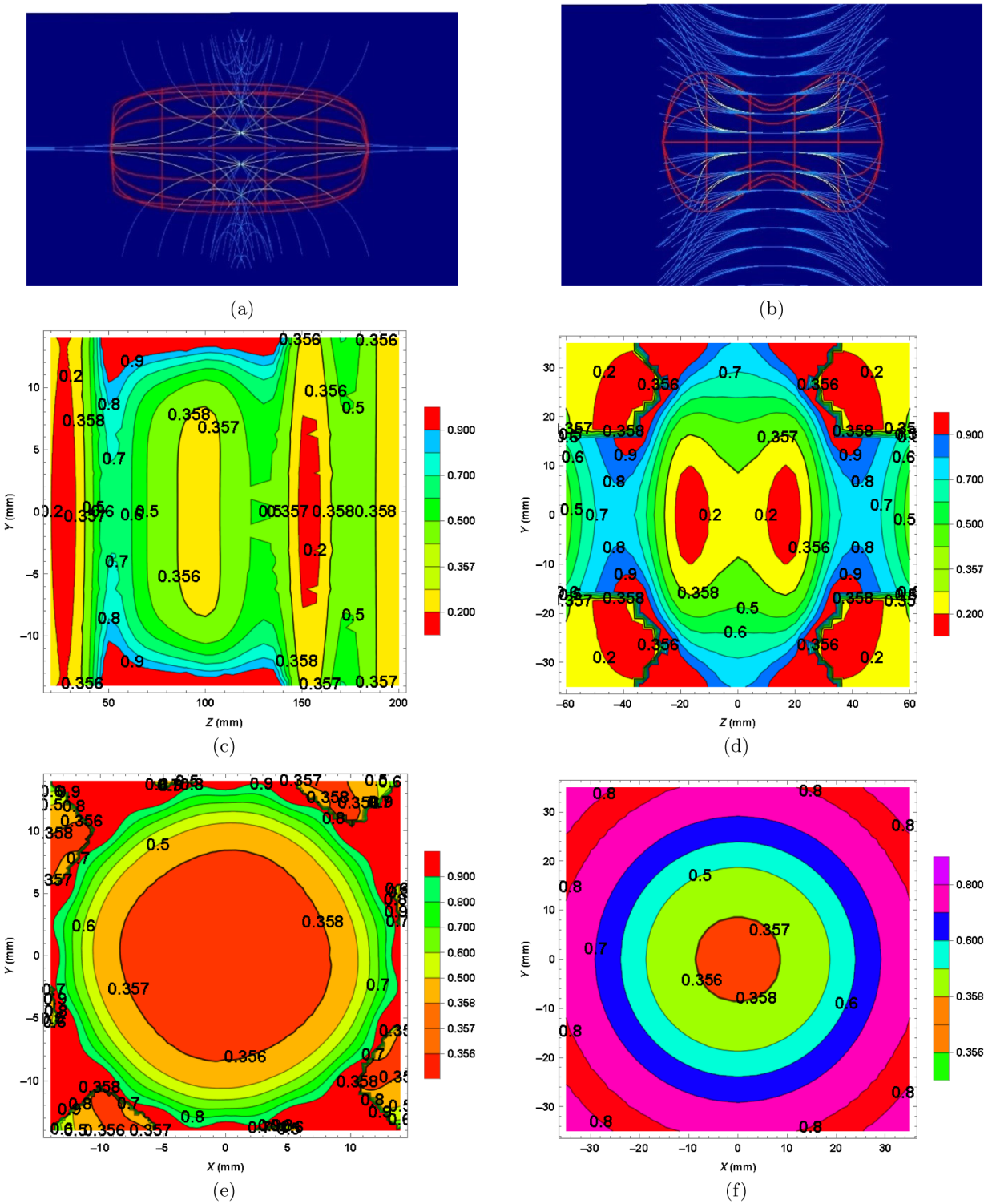

FIG. 2. Magnetic topology with resonance zone for (a) NANOGANIII and (b) PK-GANESA; Red lines belong to the ECR resonance surface, where the magnetic-field related electron-cyclotron resonance matches the microwave, namely 10 GHz; Blue lines correspond to magnetic-field lines and the yellow ones are those crossing the ECR resonance volume. Magnetic-field contour plots: in the vertical plane which contains the source axis for (c) NANOGANIII and (d) PK-GANESA; in the transverse plane at the centre of the source on the longitudinal axis for (e) NANOGANIII and (f) for PK-GANESA. The numbers correspond to the field values in T.

the centre of both sources on the source axis. Two features underline the differences: (1) the small angular dependence of the field contours of the NANOGANIII source, as compared to the axisymmetric field distribution of PK-GANESA; (2) the smaller field gradients of PK-GANESA as compared with NANOGANIII. The consequences of this specific magnetic-field structure on electron transport are evaluated in the following section with TrapCAD calculations.

II. TrapCAD SIMULATIONS

A. Simulation principles

TrapCAD [9,13,14] is a simulation tool that computes collision-less charged-particle trajectories in the ECR ion-source environment, depicted by a magnetic static field, an rf electric field (the heating microwave of arbitrary frequency and power), without considering any collisions. It also provides visualization of the trajectories as well as the possibility to sample the electron phase space as a function of time. In TrapCAD, electrons are tracked up to one of the following conditions: (1) The simulation reaches its defined maximum time; (2) electrons collide with a wall of the magnetic volume; and (3) they exit the magnetic field map through the apertures on the longitudinal axis. In the last two cases, electrons are considered as lost for the calculation.

To remain physically meaningful, i.e., to neglect effects of collisions on the electron trajectories, these calculations need to be integrated over times that are small when compared with the mean free time for electron-electron and electron-ion collisions. In typical ECR-source plasma conditions in steady-state regime, corresponding to an argon plasma with electron and ion temperatures of $T_e \sim 10$ keV and $T_i \sim 20$ eV, $n_e = 10^{11}$ cm^{-3} and a mean argon charge-state of $Z_i = 8$, the mean electron-electron Coulomb collision time is in the tens of ms range, and the mean Coulomb electron-ion collision time is $\sim$1 ms. Note that such values of the temperatures of the different species were chosen according to a preceding work [15], which used theoretical mean free-time estimates from H.I. West [16]. It is to be underlined that such values of the ion temperatures are within the range of those measured by R. Kronholm *et al.* on the 14 GHz ECR source at JYFL [17]. In that work it was found that the ion temperature depends on the charge state of the ion but rather slowly. Taking into account the dependence of the collision frequencies between the different species, we can state that we obtain the right order of magnitude for the upper bounds of these free times. Moreover, at the early beginning, the average electron energy is 10 eV with quite no ions $\langle Z \rangle \sim 0.1$ leading to an electron-ion collision time of $t = 4.4$ μs hence pure microwave heating dominates over the other collision processes.

The end time of our simulations was chosen as 20 μs to remain in the framework of a nonplasma, collisionless regime. This value has been fixed for the simulation of both sources to allow comparison. Even though this value is somewhat arbitrary, it is large enough to ensure a quantitative comparison of the performances of NANOGANIII and PK-GANESA in terms of the magnetic trapping and ECR heating of the electrons. The samples of the simulations were made of 40 000 electrons. The electrons were initially generated randomly in a volume surrounding the resonance surface. The thickness of this volume is given by a parameter ΔB (in T), which depicts a field depth around the magnetic field of the cyclotron frequency corresponding to the rf frequency (i.e., the resonance condition). The relationship between this parameter and an actual physical volume containing the resonance surface depends on the magnetic field map of the source and in particular on the shape of the resonance zone within the map. We used as a criteria to fix the value of ΔB the average kinetic energy of the electrons remaining inside the source at the end of the calculation (see Table I). The dependence of the calculation on ΔB may be explained as follows: A too-small value will select initial electrons very close to the resonance surface, favoring therefore highly accelerated electrons but for a very small part of the electron sample, as compared to the whole source magnetic volume. Such a value increases the average energy of the remaining electrons. On the other hand, a too-large ΔB will include in the simulation electrons not as efficiently heated-up by the resonance condition of the rf and hence should decrease the average value of kinetic energy of the remaining electrons. These features explain why we had to determine ΔB for each ECR source, and why we obtain different ΔB for NANOGANIII and PK-GANESA.

The initial energy of the electrons was randomly generated in the range [0–10] eV (uniform distribution). The resonant magnetic field value is 0.3751 T, corresponding to an rf heating frequency of 10 GHz, calculated from the well-known numerical formula:

$$B_{\mathrm{ECR}}[\mathrm{T}] = \frac{f[\mathrm{GHz}]}{28}. \tag{1}$$

The time step of the simulation was fixed to 3 ps. This value is the largest to give results that do not depend on it. Even for electrons of tens of keV, the step length related to it is small with respect to two typical magnetic lengths: $\langle B/\nabla B \rangle$ and the magnetic radius mv/qB_{ECR}, where m is the electron mass, v its velocity in the range of the electron

TABLE I. Simulation parameters for TrapCAD. See text for the definition of ΔB.

Ion source	Frequency (GHz)	Resonance field B_{ECR} (T)	ΔB (T)
PK-GANESA	10	0.3571	3×10^{-3}
NANOGANIII	10	0.3571	8×10^{-3}

kinetic energies considered here, q its charge, and B_{ECR} given by Eq. (1). Moreover, this provides 30-time steps in one time period of the microwave electric field. The simulations stopped after 20 μs or when all the electrons from the initial sample had exited the source chamber volume. In the following sections, three different categories of calculations are analyzed: electron energy distribution functions (EEDFs), initial and final spatial distributions of heated electrons and electron loss cones, for both ion sources.

B. Electron energy distribution functions

The electron energy distribution functions (EEDF) were determined for all the trapped electrons at 20 μs. The EEDF are shown for NANOGANIII [Fig. 3(a)] and PK-GANESA [Fig. 3(b)]. While NANOGANIII's EEDF displays a Boltzmann-like behavior $\propto \sqrt{E}\exp(-E/kT)$, PK-GANESA's one exhibits a simple exponential behavior $\propto \exp(-E/kT)$. A curve was fitted on each histogram data resulting in a temperature equivalent kT of around 6.54 keV for NANOGANIII and 2.45 keV for PK-GANESA. Thus, the average electron energy is divided by a factor of ~2.7 with respect to NANOGANIII.

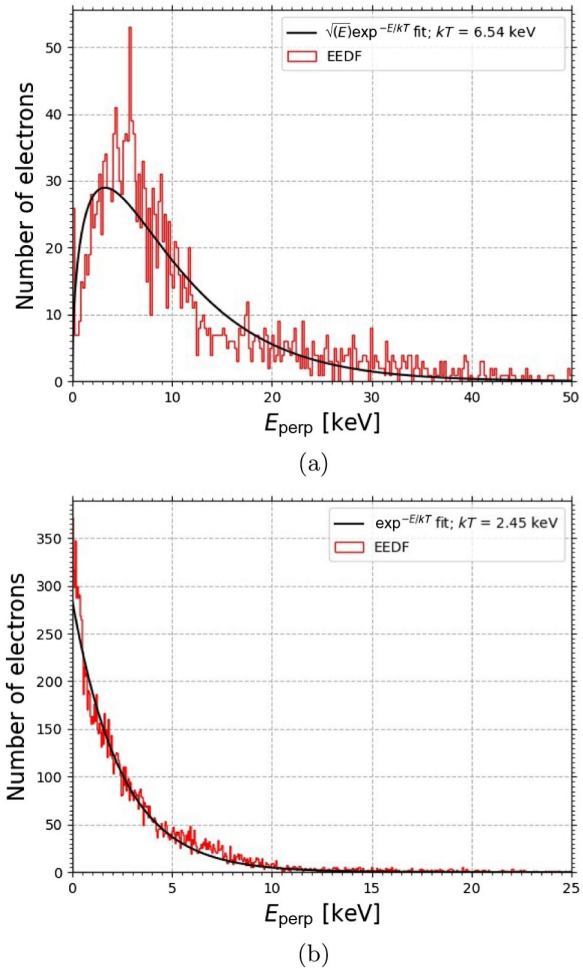

FIG. 3. EEDF of trapped electrons after 20 μs of simulation for 10 GHz 800 W rf heating (a) NANOGANIII and (b) PK-GANESA. The scale difference on the y axis is related to the numbers of the trapped electrons of both simulations [3% for (a) as compared with 30% for (b) of the same statistics of initial electrons].

The NANOGANIII EEDF has a longer high-energy tail than that corresponding to a Maxwellian distribution with a temperature of $kT = 6.54$ keV fit, meaning that electrons are trapped efficiently to experience ECR heating and reach tens of keV of kinetic energy for a sizable fraction of the electron population (over ~62 keV for the 1% of the most energetic electrons inside the distribution). In addition, there is quite a rather small number of low-energy electrons (< 1 keV), since the distribution peak is around 6.5 keV giving the clue that ECR process is effective. These low-energy electrons are quickly lost, or they gain adequate energy to be trapped and heated.

In the case of PK-GANESA, the EEDF exhibits a shorter tail, even though well above the exponential fit. The upper 1% of the distribution has kinetic energies above ~22 keV. Such a tail integral corresponds to an average energy of ~4.8 keV of an exponential distribution. However, the statistics of remaining electrons are too poor to conclude on the superposition of two exponentials in order to describe the EEDF.

Another feature of interest in the comparison of both sources is the dynamics of the rf heating with the magneto-static confinement provided by the field maps. TrapCAD keeps the information of each tracked electron until either its loss, by interaction with the source volume walls or its exit through one of the apertures of this volume (end plates, holes) or the end-time of the calculation. A possible comparison of both sources dynamics can therefore be performed by measuring the time dependence of the electron losses, over the full 20 μs simulation time, in particular as a function of the injected-rf power.

Such a dependence is displayed in Fig. 4 for three rf powers: 100, 400, and 800 W, as the integrated percentage of lost electrons from $t = 0$, when the rf heating begins. For both sources, the initial electron loss rates are very high, as the sharp increase of all curves proves it. Anyway, it should be noted that these initial loss rates are significantly much higher for PK-GANESA than for NANOGANIII. Such high rates can be interpreted by the fact that the initial electron distributions are uniform in both spatial and velocity spaces. The electrons lost in the first instants of the rf heating are those with initial velocity components within the loss cone (see Fig. 7). This difference in initial electron loss rates has therefore to be related to the differences in both magnetic field maps.

At longer timescale, the electron loss rates decrease and loss curves flatten, which is a characteristic of electron

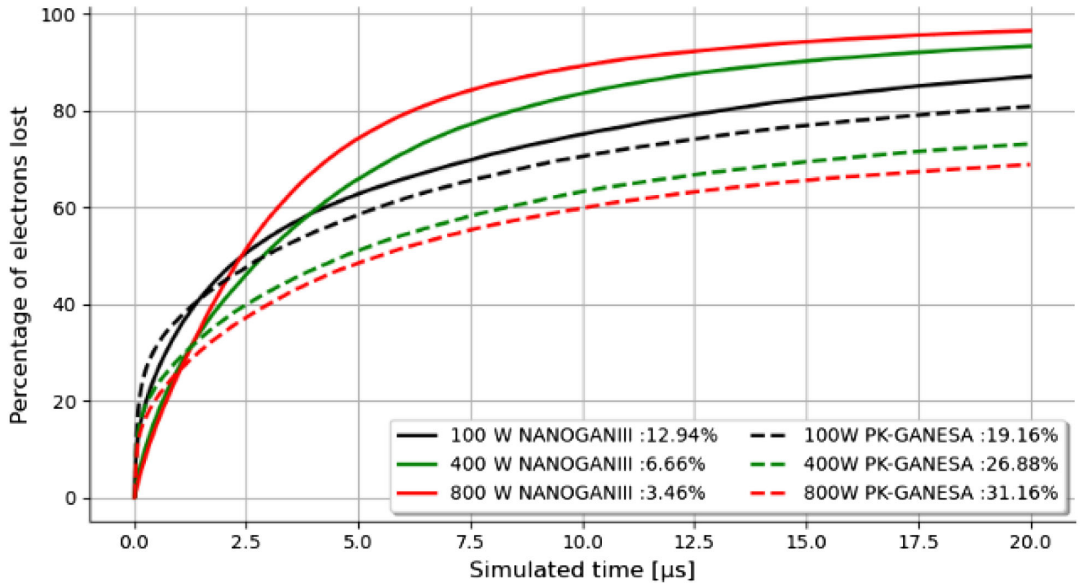

FIG. 4. Time evolution of the percentages of lost electrons (as compared with the initial statistics) for NANOGANIII and PK-GANESA at different rf heating powers. See text for the definition of lost electrons and of the initial statistics.

trapping as they are being heated. For large simulation times up to 20 μs, the curves corresponding to the two sources split into two families, with: (i) Higher loss rates on average for NANOGANIII as compared with PK-GANESA; (ii) A different rf-power dependence of both sources, with an increase in the total electron loss for NANOGANIII as rf-power increases and a decrease for PK-GANESA.

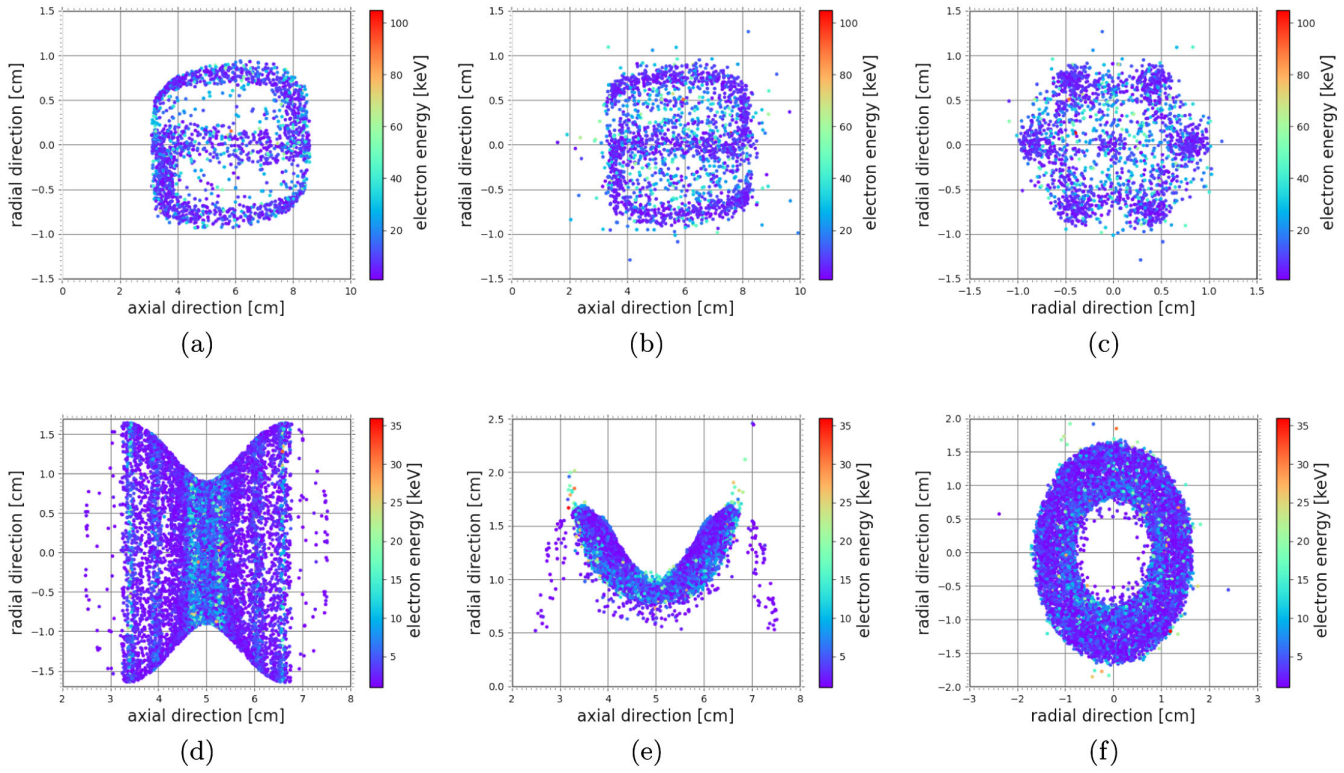

FIG. 5. Electron spatial distribution of nonlost (trapped) electrons at 20 μs: (I) NANOGANIII (a) initial position, (b) final position, and (c) radial view; (II) PK-GANESA (d) initial position, (e) final position, and (f) radial view.

At 800 W, NANOGANIII has lost 97% of the initial electron sample at 20 μs, whereas PK-GANESA 70% only. There is hence an order of magnitude higher population of trapped electrons in PK-GANESA than in NANOGANIII. Moreover the difference of behavior of the electron losses with increasing rf power of the two sources should be underlined: Losses increase for NANOGANIII, whereas they decrease for PK-GANESA. This trend should be related to the evolution of the EEDF of the remaining electrons which is pushed toward higher energies in average, with a population of remaining low-energy electrons going toward 0 [18]. This nontrivial dependence is uneasy to explain, since it goes against expectations. But this can be put in parallel with two other results of our simulation. The first, underlined above is the high initial electron loss-rate of PK-GANESA, i.e., at times when almost all electrons have a low kinetic energy. This variation goes along with a faster decrease of this loss-rate at higher power than at lower (see Fig. 4). The second result to be mentioned here is that the shapes of the EEDF of both sources do not change with the rf power in the domain we studied, from 100 to 800 W, only the temperatures increase. It looks therefore like the PK-GANESA magnetic trap is all the more efficient as the electrons are heated more quickly. This has to be related to the differences of the field-line topologies of the two sources. Looking at Figs. 2(a) and 2(c) we note that within NANOGANIII's magnetic volume, there are field lines connecting the inner part of that volume to the exits, which can be followed by the heated electrons. At variance, when heated electrons are trapped in the field lines of PK-GANESA, which remain parallel to the source axis, they cannot drift magnetically toward the exits. And as will be discussed below, the main difference between both sources as far as the electron transport at long times is concerned is that in NANOGANIII a large part of the initial electrons are lost through the magnetic volume aperture, contrary to PK-GANESA for which this part is very small (see Fig. 7 below). We can therefore conclude on a more efficient trapping of heated electrons in PK-GANESA than in NANOGANIII.

TrapCAD provides the final positions of the trapped electrons after the simulation is stopped. This has been visualized in the form of a density color scatter plot showing the final spatial distributions. For NANOGANIII, it reveals a familiar star shape with energetic electrons populating the arms of the sextupole ending on the source axis [Figs. 5(a) and 5(b)]. Similar trends have been observed in previous numerical simulations of ECR plasma by Mironov *et al.* [19]. Such similarities, as a benchmark of our simulation, give a strong basis to analyze the results obtained with PK-GANESA. The axisymmetric nature of this latter source permits to superimpose the electron spatial distribution plot along the symmetry axis [Fig. 5(c)] and in the plane transverse to the symmetry axis [Fig. 5(d)]. The final spatial distribution of the trapped electrons reveals a banana-shaped zone, in the middle of the plasma chamber along the longitudinal axis, but off the axis in the transverse plane (no electrons below $r = 5$ mm), which contains most of the energetic electrons as indicated by the presence of "green-colored" electrons having energies equal to or greater than ∼5 keV. When correlating these electrons to their initial positions [Fig. 5(f)], it appears that electrons originating in the central throat and thin strips along the bulbs get heated up the most. For comparison, we also provide the initial distribution of the nonlost electrons for NANOGANIII in Fig. 5(e).

The loss cone for both ion sources are shown on a $v_\perp$ versus $v_\parallel$ graph (electron velocity perpendicular and parallel to the magnetic field) [20] (Fig. 6). The calculations

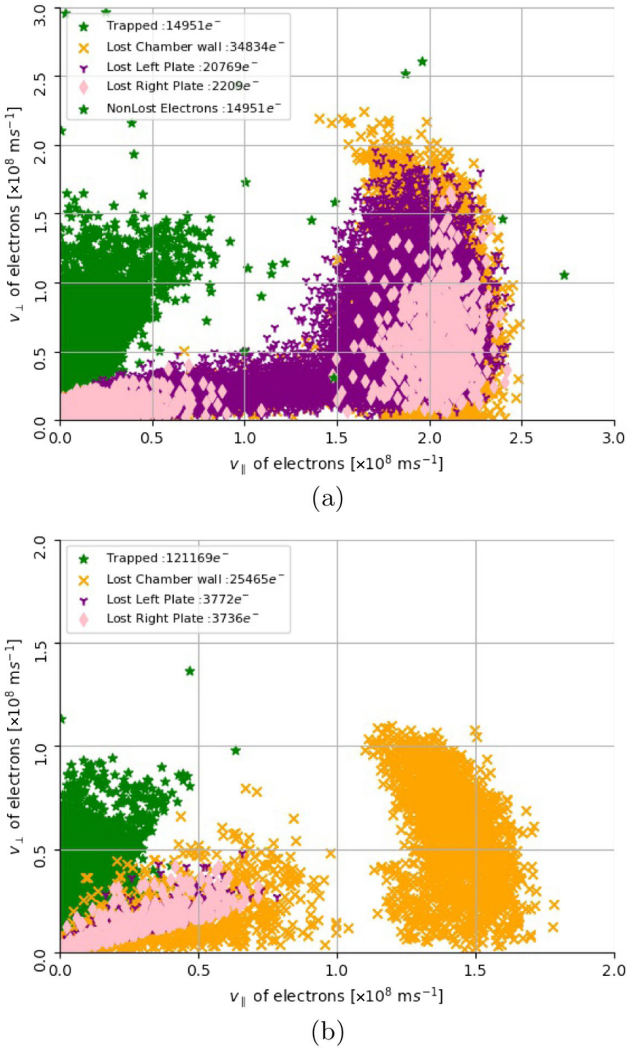

FIG. 6. Loss cone, at 10 GHz 800 W rf heating for (a) NANOGANIII and (b) PK-GANESA; the green points represent trapped electrons and the purple, pink, and orange represent lost electrons to the left side, right side, and chamber walls, respectively. Each point represents an electron of the statistical sample.

have been made for the final electron energies after 20 μs and 10 GHz, 800 W ECR heating or their energies when they were lost in the simulation. The loss cone comes from the pitch angle which is the angle between $v_\perp$ and $v_\parallel$. This defines the conditions required for successfully trapping the electrons: Electrons must have a perpendicular velocity larger than the parallel velocity. The data for the plot were obtained by numerically treating the final energies of the electrons from the output files of TrapCAD, to obtain the velocities. These data were visualized using a scatter plot with each point representing an electron. The pitch angle can be calculated using the formula:

$$\Theta_0 = \arcsin\left(\sqrt{\frac{B_{\mathrm{ECR}}}{B_{\mathrm{max}}}}\right). \tag{2}$$

Using Eq. (2) on measuring the pitch angle for NANOGANIII, $\Theta_0 \simeq 43°$ from Fig. 6(a) along with $B_{\mathrm{ECR}} = 0.3751$ T, we obtain $B_{\mathrm{max}} \simeq 0.806$ T, which is equal to the actual maximum magnetic field strength for NANOGANIII $\simeq 0.8$ T. This provides us with a way to affirm our results from the simulations. The scatter plot also shows that the number of electrons lost on the right plate is smaller than that on the left plate. This is linked to the extraction on the left side, requiring a lower maximum magnetic field lower as compared with the right side. On measuring the pitch angle for PK-GANESA [Fig. 6(b)], $\Theta_0 \simeq 38°$ and with $B_{\mathrm{ECR}} = 0.3751$ T, we get $B_{\mathrm{max}} \simeq 0.989$ T which is close to the actual magnetic field strength of $\simeq 1$ T. That corresponds to almost the last closed iso-module of the magnetic field map. The lost electrons are identical for the right and left sides, respectively, due to the actual left-right symmetry of the ion source magnetic poles' geometry. For PK-GANESA, we have separated the lost electrons into two populations below or above 12 keV of final kinetic energy. This value was chosen because it divides the sample of lost electrons in two separated populations in the $(v_\perp, v_{//})$ phase space. When considering the initial spatial distribution of these electrons (Fig. 7), we see that they originate from the middle throat and thin strip zones near the bulb, similar to the trapped electron positions [Fig. 5(d)]. This shows that electrons from certain initial spatial regions of the resonance zone are more heated as compared to others.

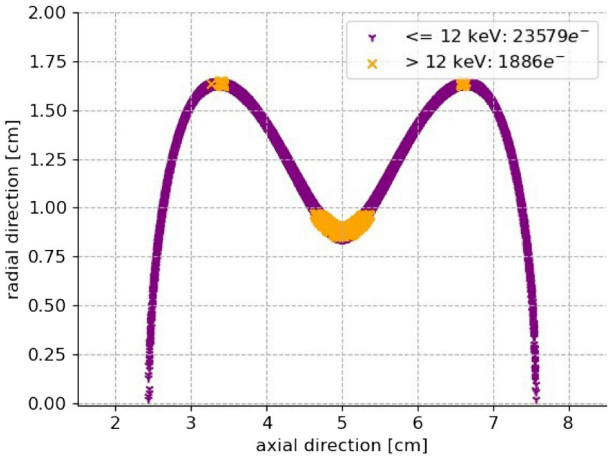

FIG. 7. Initial spatial distribution (x coordinate: symmetry axis of the source, y coordinate: transverse radius) of lost electrons with two different ranges of energies corresponding to Fig. 6.

III. SIMION SIMULATIONS

The above analysis indicates that the rf-heating dynamics are in principle favorable for the production of HCS ions in PK-GANESA. In the present study and in order to attempt an explanation of the measured differences of ion-charge spectra between NANOGANIII and PK-GANESA, we have tested the following hypothesis: HCS ions are indeed produced with PK-GANESA in volumes where hot electrons are confined but are unable to escape the source inner volume through the exit aperture on the symmetry axis. For such a test, we have employed the SIMION simulation package [10]. SIMION has been developed to calculate charged-particle tracks (both electrons and ions), once the rf electric field, electrostatic, and/or magnetostatic field maps are defined.

We used the final electron spatial distribution, with the hypothesis that the HCS ions will be generated in regions where high-energy electrons are confined. The ions simulated were $^{40}Ar^{1+}$ and $^{40}Ar^{8+}$ ions. We generated 500 ions in the chamber with 1 eV energy to gather crude statistics for the two ion species. The simulations revealed that none of the 8+ ions could escape through the extraction port and if we let the simulation run long enough, they are either trapped and the calculation is stopped by SIMION or they are lost on the chamber wall. The simulations have been initiated from the inner region as well as the extreme outer region of the magnetic trap facing the extraction port. As the electrons in the outer locations display a lower-energy content with an average energy of 0.16 keV, only low-charge states might be produced. In that framework, 1+ ions are generated and actually can escape, to be extracted. In our simulation, only 13 of the generated 500 ions were computed. This means that only 13 of the 500 ions were able to escape from the extraction port and the rest were lost to the chamber walls. Figure 8 shows ion trajectories computed with SIMION: In Fig. 8(a), Ar^{8+} are trapped inside the magnetic field distribution; in Fig. 8(b), a part of the Ar^{1+} ions produced close to the exit of the magnetic volume can escape toward the extraction line.

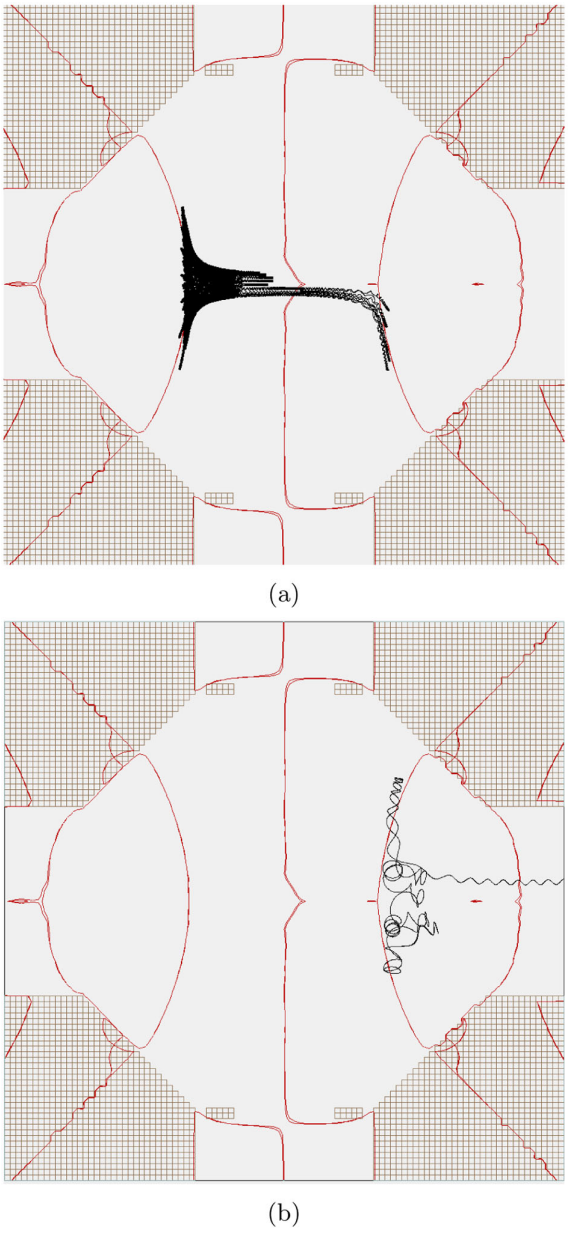

FIG. 8. Trajectories computed with SIMION. (a) $q = 8$; (b) $q = 1$. Ar^{8+} ions are trapped inside the magnetic field distribution.

IV. CONCLUSIONS

The PK-GANESA ion source was designed with a new magnetic-field structure, fully axisymmetric in order to improve the matching of the exiting ion flux with the acceptance of an ion-accelerator injector [5]. Rather unexpectedly, the first measurements with this source have shown that only low-charge state ions ($\lesssim 4$) could be extracted from the source, at variance with, e.g., the more conventional-design NANOGANIII ion source [3].

Prior to a full plasma simulation, we studied the dynamics of electron heating in PK-GANESA with the collision-less tracking simulation-tool TrapCAD. In order to be able to draw meaningful conclusions from our analysis, we performed the same calculations for the NANOGANIII ion source with the goal of comparing both sets of results.

This comparison shows essentially that for long times, defined here as $t = 20$ μs: (i) The average kinetic energy of the remaining electrons is higher in NANOGANIII than in PK-GANESA; (ii) the proportion of remaining electrons from the initial electron sample is higher for PK-GANESA than for NANOGANIII by one order of magnitude at 800 W rf power. The combination of both results leads to the conclusion that the confinement of hot electrons is more efficient in PK-GANESA as compared with NANOGANIII. This should in principle translate into a higher current exiting PK-GANESA than exiting NANOGANIII for a given ion charge state, observed at low charge-states but not at high-charge states (HCS).

To make a step further in our study, we performed a simulation of the ion transport in the magnetic field map of PK-GANESA with SIMION. This showed that HCS ions, if produced in the region corresponding to the magnetic confinement of hot electrons as computed with TrapCAD are themselves confined in this magnetic structure and unable to escape through the plasma electrode aperture along the symmetry axis of the source, whereas 1+ ions can, fully in agreement with what was measured.

The above conclusions must be softened by the fact that they came up from a numerical study without collisions and in a timescale domain much smaller than a steady-state plasma operation. The EEDF will be modified [21] as soon as collisions occur leading to the arisen question: Will the EEDF still include enough electrons with energies in the keV range to produce HCS continuously?

For that reason, the next step in this work is to perform full fluid/hybrid or particle-in-cell (PIC) simulations for the PK-GANESA ion source and to test our assumption of ion production and trapping. In parallel, we plan to investigate the ion source behavior with selective diagnostics such as optical emission and Bremsstrahlung-photon spectroscopy or incoherent Thomson scattering. The ion source also requires a dedicated setup for ion exhaust, to transport the ions on axis to be able to extract them. This is presently being studied.

[1] A. C. C. Villari, The accelerated ISOL technique and the SPIRAL project, Nucl. Phys. **A693**, 465 (2001).
[2] N. Alahari and H. Goutte, Microscopes for physics at the femtoscale, Nucl. Phys. News **31**, 5 (2021).
[3] R. Leroy, C. Barué, C. Canet, M. Dubois, M. Dupuis, F. Durantel, J.-L. Flambard, G. Gaubert, S. Gibouin, and C. Huet-Equilbec, Ion sources at GANIL, in *Proceedings of the 17th International Conference on Cyclotrons and their applications, Tokyo, Japan* (Saitama University, Institute

of Physics and Chemistry Research Cosmic Radiation, Saitama, 2005).

[4] R. Geller, *Electron Cyclotron Resonance Ion Sources ECR Plasma* (IOP Publishing Ltd., London, 1966).

[5] P. Salou and L. Maunoury, PK-GANESA: An ECRIS for testing the axisymmetric magnetic structure for the production of multicharged ion beams, AIP Conf. Proc. **2011**, 040021 (2018).

[6] P. Jardin, C. Barué, C. Canet, M. Dupuis, and J. L. Flambard, Mono 1000: A simple and efficient 2.45 GHz electron cyclotron resonance ion source using a new magnetic structure concept, Rev. Sci. Instrum. **73**, 789 (2002).

[7] O. Tuske and L. Maunoury, Visible light spectrometry measurements for studying an ECRIS plasma and especially applied to the MONO1001 ion source, Rev. Sci. Instrum. **75**, 1529 (2004).

[8] G. Gaubert, Réalisation d'un banc de tests de sources d'ions, Training report for CNAM Engineering diploma (2004).

[9] J. Vámosi and S. Biri, TrapCAD—a tool to design and study magnetic traps of ECR ion sources, Nucl. Instrum. Methods Phys. Res., Sect. B **94**, 297 (1994).

[10] David D. Dahl, SimION for the personal computer in reflection, Int. J. Mass Spectrom. **200**, 3 (2000).

[11] P. Spädtke, R. Lang, J. Meder, J. Rodfbach, and K. Tinschert, Low energy beam transport for ion beams created by an ECRIS, in *Proceedings of ECRIS, Chicago, IL* (JACoW, Geneva, 2008), https://accelconf.web.cern.ch/ecris08/INDEX.HTM.

[12] P. Spädtke, R. Lang, J. Meder, F. Maimone, J. Rodfbach, and K. Tinschert, Ion beam extraction from magnetized plasma, in *Proceedings of ECRIS, Sydney, Australia* (JACoW, Geneva, 2012), https://accelconf.web.cern.ch/ECRIS2012/papers/proceed.pdf.

[13] J. Vámosi and S. Biri, TrapCAD—A program to model magnetic traps of charged particles, Comput. Phys. Commun. **98**, 215 (1996).

[14] S. Biri, A. Derzsi, É. Feket, and I. Iván, The upgraded TrapCAD code, J. High Energy Phys. Nucl. Phys. Chinese Edition Suppl. **31**, 165 (2007).

[15] L. Maunoury, C. Pierret, S. Biri, and J.-Y. Pacquet, Studies of ECR plasma using TrapCAD code, Plasma Sources Sci. Technol. **18**, 015019 (2009).

[16] H. I. West, Lawrence Livermore National Laboratory Intern. Report No. UCRL-533391, 1982.

[17] R. Kronholm, T. Kalvas, H. Koivisto, J. Laulainen, M. Marttinen, M. Sakildien, and O. Tarvainen, Spectroscopic study of ion temperature in minimum-B ECRIS plasma, Plasma Sources Sci. Technol. **28**, 075006 (2019).

[18] A. Khandelwal, Master 2 Internship Report GANIL (2021).

[19] V. Mironov, S. Bogomolov, A. Bondarchenko, A. Efremov, and V. Loginov, Spatial distributions of plasma potential and density in electron cyclotron resonance ion source, Plasma Sources Sci. Technol. **29**, 065010 (2020).

[20] O. Tarvainen, Studies of electron cyclotron resonance ion source plasma physics, Ph.D. dissertation, University of Jyvaskyla, 2005.

[21] V. Mironov, S. Bogomolov, A. Bondarchenko, A. Efremov, and V. Loginov, Some aspects of electron dynamics in electron cyclotron resonance ion sources, Plasma Sources Sci. Technol. **26**, 075002 (2017).